Impact of the Seed Layer Morphology on the Initial Growth of HPMC-Si Ingot

Giri Wahyu Alam, Etienne Pihan, Benoit Marie, Nathalie Mangelinck-Noël

Impact of the initial growth interface on the grain structure in HPMC-Si ingot

Giri Wahyu Alam[1,2,3,], Etienne Pihan[1], Benoit Marie[1], Nathalie Mangelinck-Noël[2]

[1] Univ. Grenoble Alpes, INES, CEA, LITEN, Department of Solar Technologies, F-73375 Le Bourget du Lac, France

[2] Aix-Marseille University, CNRS, IM2NP, UMR CNRS 7334, Campus Saint-Jérôme, Case 142, 13397 Marseille Cedex 20, France

[3] Centre of Technology for Materials, Agency for the Assessment and Application of Technology, Bldg. 224 PUSPIPTEK, South Tangerang 15314, Indonesia

***Abstract* — In High Performance Multi-Crystalline-Silicon (HPMC-Si) ingots, small seed grains generate grain boundaries that can terminate the propagation of dislocation clusters. Here, we focus on the seed template formation and its impact on the initial growth by directional solidification utilizing metallography, photoluminescence, and EBSD analysis. In the seed region, two randomly oriented grain morphologies are found: a genuine non-melted seed from the poly-Si chunks, and a re-solidified infiltrated molten silicon region. All grains grow by epitaxy on the seed grains and grains grown from wider grains in the seed, reach a higher solidification height.**

***Index Terms* — EBSD, grain structure, HPMC-Si, photoluminescence, seeded growth.**

I. Introduction

In both research and industry, seeding is an explored way to control the final structure of Silicon photovoltaic (PV) ingots. In particular, HPMC–Si method makes use of fine grained seeds aiming at creating grain boundaries that can terminate the propagation of dislocation clusters [1-3]. Indeed, dislocation clusters coupled to impurities are very detrimental to PV properties [4] so that it is necessary to limit their propagation. Numerous characterization studies concerning the grain morphology during ingot growth have led to the conclusion that RAGB presence in the growth area and small grain size are of primary importance to provide sufficient termination sites for dislocations clusters [5]. Consequently, the crystalline defect density in the growth ingot can be reduced. However, initial growth on seeds and seed morphology has only been studied in details by few authors. Ronit *et al.* [6] describe the growth from poly-Si seeds as a three stage process. Those authors evidenced an initial growth with spherical grain morphology (stage I), from which grains grow in the solidification direction together with grain selection (stage II) before to reach a steady state in terms of columnar grain size (stage III). From the observation of the grain structure in both FBR (Fluidized Bed Reactor) and poly-Si seeds, Ekstrøm *et al.* [7] observed a coarsening of the microstructure of the two seed materials. In the case of poly-Si chips, the authors also observed a larger grain structure initiated from silicon infiltrated in-between poly-Si chunks gaps below the main seed interface.

It is the aim of this contribution to deepen the knowledge of initial grain template formation in seeds and to discuss its consequences on initial grain structure at the start of HPMC-Si ingot growth. The ultimate objective is to tailor the seed layer morphology to control the final grain structure. As a consequence, we focused on metallographic observations, photoluminescence imaging, etch pits analysis and EBSD mapping of:

- initial seed layer composed of poly-Si chunks grain structure and inter-chunks gaps,
- seed layer formation from genuine non-melted seed from the poly-Si chunks and from re-solidified infiltrated molten silicon,
- grain structure in the vicinity of the seed / initial growth interface.

II. Experimental Techniques

A G2 (60kg) silicon ingot was directionally solidified from high purity (> 250 Ω.cm) WACKER poly-Silicon (Size 4) in a silicon nitride coated VESUVIUS silica crucible. Boron doped silicon was added close to the top of the poly-Si chunks to achieve 1 - 2 Ω.cm resistivity target. The melting and growth interface was concave and a dipping rod provided regularly the information on residual solid height in the middle of the ingot. The seed arrangement consisted of 20 mm poly-Si chunks Size 1 (length range 0 – 15 mm chunk size). During the melting segment, the top and bottom zone temperatures were set at 1510°C and 1410°C, respectively while the growth rate was set at 1.2 cm/h. The position of the sample extracted from the ingot and studied in details in the following can be seen in red Fig. 1. This sample is situated at the seed layer- initial growth interface in a region of concavity of the solid/liquid interface. Besides, a reference sample (30 mm in diameter) was created by introducing Epoxy Araldite AY-103 resin in size 1 poly-Si chunks to simulate the initial seed morphology and to observe initial grain size and gaps between chunks.

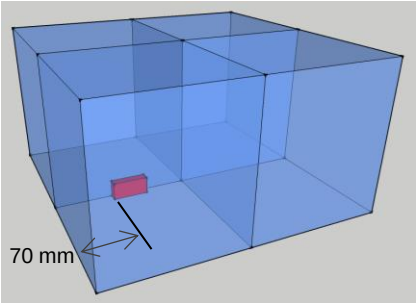

Fig. 1. Position of the sample inside the ingot (red parallelepiped).

After polishing, the selected sample was characterized using photoluminescence (LIS-R2-[8]) to identify seed layer-initial growth interface from doping variation influence on carrier density under illumination. Etch pit studies were performed using Wright etchant [9] to reveal dislocations and grain boundaries. Lastly a SEM – Nova Nanosem 630 was used for EBSD mapping with a 9.9 µm step on a selected 10 x 8.85 mm^2 area across the seed-initial growth interface to study grain structure and crystallographic orientation.

III. ANALYSIS OF THE RESULTS

A. Initial seed layer

The reference sample was observed during resin pouring. There were many gas bubbles escaping from the gaps simultaneously to the resin filling in the gaps between poly-Si chunks. Gas pockets were trapped and concentrated on the isolated areas between the stacked poly-Si chunks or are due to its irregular shape. After resin hardened, it was horizontally polished and vertically cut in the middle revealing the cross section of the poly-Si chunks. Gap widths between poly-Si chunks are found highly variable in the range of 0.1 mm to 15 mm horizontally and 0.06 mm to 7.3 mm vertically. At the same time, the cross section of poly-Si chunk can be very thin around 0.09 µm in thickness.

Metallography of the initial poly-Si chunks reveals two main microstructure morphologies and are measured by Abrams Three-Circle Procedure (Fig. 2) [10]: isolated concentric columnar grains with grain size over 10 µm, some even reaching 150 µm (red arrows) and abundant small elongated grains, below 10 µm diameter (yellow arrows). Concentric columnar grains are also found in [11] and are called "feather" like structure. This measurement is comparable to the measurement in [11] that used Heyn Intercept Method with a circular line. Additionally, many circle shape defects (yellow rectangle) which, behave as cracks in the chunks are observed on the surface. Their origin is unknown to the authors. Dislocation etch pits are found in all grains of the initial poly-Si under 500x magnification and above. Moreover, Σ3 twins are revealed particularly in the large columnar grains.

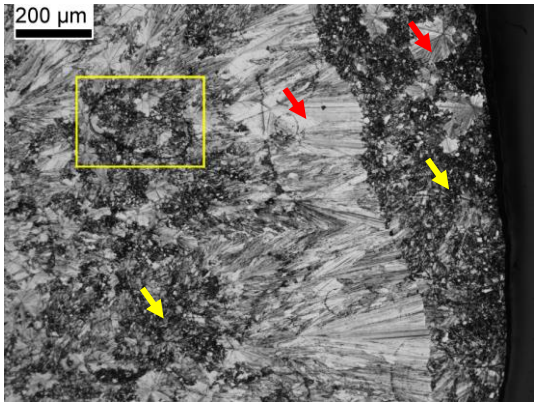

Fig. 2. Reference typical initial poly-Si microstructure (polished and wright etched reference resin infiltrated sample).

B. Seed layer in the grown ingot

PL imaging (Fig. 3) allows identifying precisely the position of the concave initial growth interface separating seed layer (darker bottom domain) and growth (light grey top domain) at the beginning of the process. The unambiguous use of PL is probably related to the different doping concentrations in the seed layer region and in the molten silicon just before the crystallization started. The observation of very bright domains near the growth interface is an indication that dopants are imbedded in the re-solidified areas in the seed layer during the early stages of the melting segment. However, it must be reminded that the PL contrast reveals a complex combination of doping and crystalline quality in the sample. The growth interface is found almost continuous separating spherical and columnar grain structures.

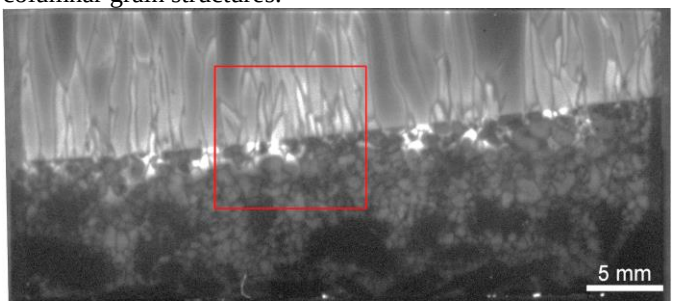

Fig. 3. Photoluminescence imaging using high magnification lens at the bottom of the grown ingot (40x20 mm^2) showing both seed layer and growth areas delineated by the initial growth interface.

In Fig. 3, the genuine non-melted seed domains and the re-solidified infiltrated melt domains are revealed by a dark PL intensity and a brighter PL intensity, respectively. Similarly to the reference sample, the gap width between non-melted chunks is around 10 mm at maximum.

Chemical etching of the same area (Fig. 4) allows to identify the associated morphology. One can distinguish two main grain structures and two sublayers in the seed layer. From the interface to a position about 4 mm below it, most of the grains have an aspect ratio close to unity. Below that level, we clearly distinguish genuine non-melted seed domain of poly-Si chunks (size < 200 µm) from re-solidified infiltrated melt domains (size

472 µm in average and Coefficient of Variation (CV) 0.37) [12].

Moreover, we can see in Fig. 4 that genuine non-melted seed from poly-Si chunks undergoes a strong grain coarsening generating an increasing grain size toward the growth interface (from 18 – 72 µm at the seed layer bottom to around 300 µm close to the initial growth interface), everywhere far above the initial grain size.

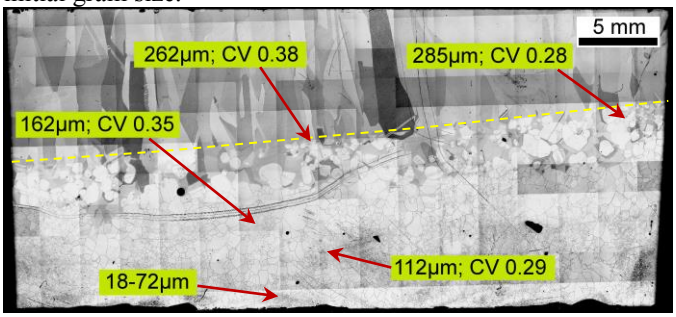

Fig. 4. Build-up of the same area as in Fig. 3 (optical images after chemical attack). The yellow dashed line delineates the initial growth interface determined from PL. Local grain size in genuine non-melted seed are also indicated.

C. *Grain structure in the vicinity of the seed layer-growth interface*

The 10 x 8.85 mm2 area identified as a red box in Fig. 3 was analyzed in more details using EBSD (Fig. 5). The EBSD technique provides both crystallographic orientation (IPF: Inverse Pole Figure, Fig. 5a) and grain boundary types (Fig. 6a).

At first, EBSD results also confirm that all grains from the seed intersecting the initial interface grow as columnar grains due to the directional solidification process. Second, regarding grain size and morphology measured from Heyn Lineal Intercept Method with straight lines [10] and aspect ratio, it appears that:

- the seed layer up to 4 mm below the initial interface position (Fig. 5a) has an average grain size of 465 µm (CV 0.78) and 453 µm (CV 0.94) in the horizontal and vertical directions respectively. The average aspect ratio is around 1 indicating spherical grains in longitudinal sections.
- columnar grains above the initial interface position (Fig. 5a) grow on seeds with an average grain size of 352 µm (width) near the seed layer-initial growth interface line.
- the average width almost doubles to reach 639 µm after 5 mm of growth on the top side of observed area indicating strong grain selection in the very first 5 millimeters of growth

Both morphologies of seed grains (spherical and columnar) have a random orientation as shown in Fig. 5a. In the growth region just above the interface (Fig. 5c), the crystallographic orientations along the growth direction are mostly in direction near-<115> and nearly none near-<101> and <111>. The texture in the initial growth region (Fig. 5b) and seed layer (Fig. 5c) are not identical due to the fact that the orientations of the grains in the seed region are not all present at the level of the initial growth interface.

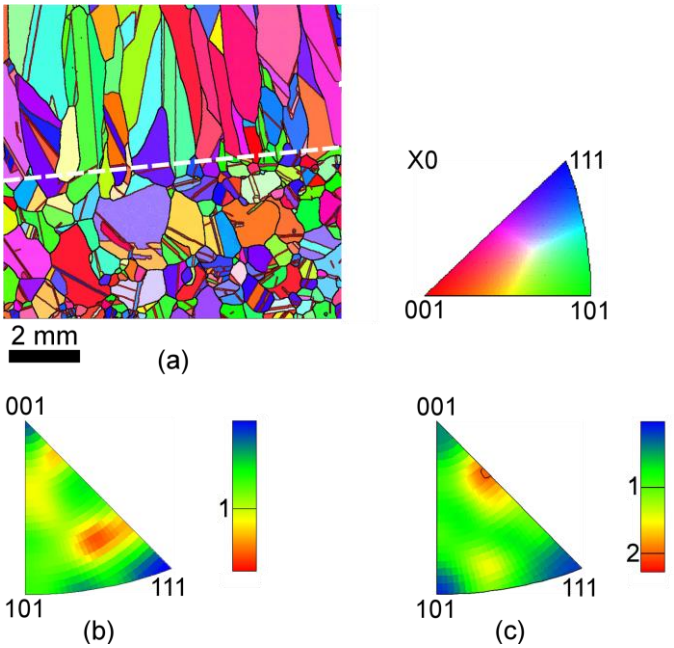

Fig. 5. (a) EBSD IPF (Inverse Pole Figure) map along the growth direction X0. Texture of the seed layer area (b), and of the initial growth area (c).

To understand in deeper details the grain formation and competition from the seed, we measure the growth length of the different grain boundary types. In our process, the length percentage of RAGBs (Fig. 6b) is the highest then followed by Σ3, Σ9, Σ27a, and Σ27b length percentage. The growth lengths of Σ9, Σ27a, and Σ27b are the smallest. These observations confirm that grains start there growth by nucleation on the

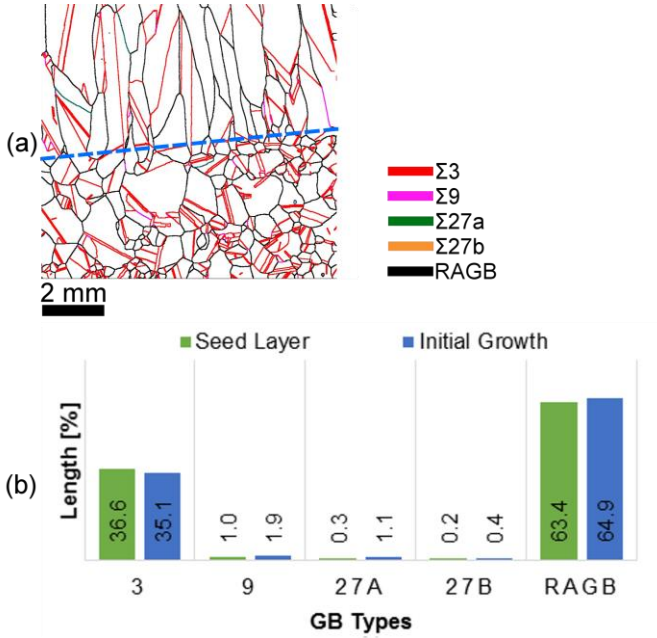

Fig. 6. The grain boundary map showing selected twin grain boundaries (Σ3, Σ9, Σ27a, Σ27b) and RAGB (a) and Length proportion of each grain boundary types in the seed (green) and growth (blue) regions just above the initial interface (b).

randomly oriented seed grains leading to a randomly oriented grain structure at the beginning of growth. This is consistent with the lower occurrence of Σ3 grain boundary type. Another study will be devoted to the evolution of the grain structure upper in the sample where Σ3 grain formation followed by the formation of Σ9, Σ27a, and Σ27b by competition could be expected [13] oppositely to random nucleation.

Measuring the grain width at the level of the initial growth interface shows that the grain width is linked to the columnar grain propagation length. In the EBSD observation area, about 50% of the grains have a width between 200 – 400 µm, and the rest have a width between 400 – 1200 µm.

The growth length of columnar grains issued from a grain width lower than 400 µm is below 1 mm for 70% of them and none reaches a growth length of 3 mm. In the case of grains with an initial width higher than 400 µm, there is no stop of growth before 1 mm, around 20% does not reach a higher growth length than 2 mm and 40% reaches a growth length above 4 mm.

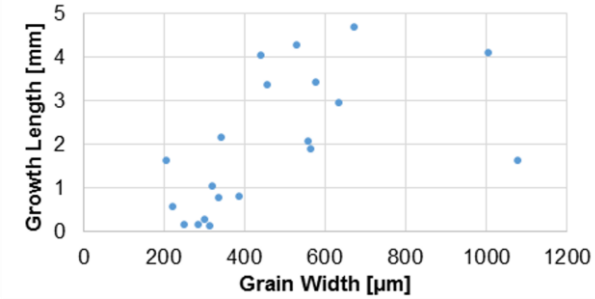

Fig. 7. Growth propagation length perpendicularly to the interface as a function of grain width measured at the initial interface from Fig. 5.

IV. Discussion

A. *Formation of the seed layer*

During the resin pouring, the resin easily reached the bottom of the mold and filled in the gaps between the chunks. The viscosity of this resin (1800 – 2400 mPa.s at 25°C [14]) is higher than the molten silicon viscosity at the melting point (0.575 mPa.s [15]). As a consequence, we can conclude that the molten silicon can flow down and fill in the seed layer gap without retardation and can finally reach the bottom surface of the crucible. In parallel, there is an intense exchange in the seed layer between the argon gas that previously fills the gap between the poly-Si chunks and the infiltrated molten silicon. However, this exchange cannot completely be carried out in some areas because the escaped gas can be trapped in between the stacked chunks, thus creating gas holes as also observed in metal casting. The cavities are not always caused by the trapped gas. Indeed, due to the heat distribution in the seed layer, a colder area in the corner crucible of a concave furnace type is created. When approaching this area, the temperature of flowing molten silicon reduces rapidly and might freeze before completely filling the seed layer gap.

Our results in Fig. 3 and Fig. 4 show that, on the one hand, some large spherical grains (499 µm (CV 0.68) in average) grow during the melting stage inside the seed layer gap and that on the other hand, poly-Si coarsening is significant (from size lower than 100 µm to grain size larger than 200 µm). In the following, the first and the second regions are denoted respectively re-solidified infiltrated molten silicon and genuine non-melted silicon. The first region is created after the infiltrated silicon is accumulated in the bottom crucible and re-solidified between the poly-Si chunks. The low temperature difference and the higher solidification rate creates re-solidified grains with an aspect ratio close to 1. In average, these grains have a bigger size than the second region of genuine non-melted silicon at the bottom crucible. This phenomenon is also discussed in [16, 17].

The falling molten silicon corresponds to the first silicon melted and can be doped with various amounts of dopants depending on its initial location in the crucible. Indeed, Boron doped silicon was initially situated at the top part of the feedstock arrangement. As a consequence, it is believed that the varying PL contrasts in the seed layer in (Fig. 3) is due to successive melt infiltrations downwards in the gaps even though, the PL contrast can also indicate a defective area. Upon measuring the resistivity, the target value of 1 – 2 Ω.cm in the whole ingot growth is attained only from the middle height of the ingot growth. It implies that some dopant still remains somewhere in the seed layer after the melting segment ends. As a consequence, the molten silicon has a lower than expected concentration of boron in the initial growth.

In the vertical direction, the seed layer structure can be divided in two main regions: re-solidified infiltrated molten silicon and genuine non-melted silicon.

In parallel, the applied thermal gradient also creates conditions for grain coarsening inside the seed. A strong grain coarsening on the genuine non-melted seed increases the seed grain size. The very dark PL intensity as found on the bottom crucible is to be related to a smaller grain sizes and a high etch pits density. When grains reach a specific size (> 300 µm), their emitted PL intensity is similar as the one from re-solidified infiltrated molten silicon. This condition is observed in the seed layer up to 4 mm below the growth interface. Consequently, it is difficult to distinguish between grains originating from solidified infiltrations in-between the seed chunks (~ 500 µm) and large coarsened grains of poly-Si chunks (> 200 µm). However, some genuine non-melted seed is still present close to the interface as indicated from the circular crack in poly-Si chunk also evidenced in the literature [7] and from the dark PL intensity region for different experimental conditions.

Moreover, comparison to the grain structure in the seed layer of another run, with different thermal history during the melting segment, shows that genuine non-melted seed of poly-Si grain coarsening is dependent on thermal history during the melting segment. The grain coarsening might start from the beginning of the melting segment, i.e. earlier than in the case of the

infiltrated molten silicon, as long as the poly-Si chunk temperature reaches 1000°C or 1150°C [10, 18]. At this temperature, the grain coarsening could be generated gradually from the poly-Si chunk surface towards the center depending on the heat on its surface. The thickness of the poly-Si chunk might also induce a temperature difference between the surface and the inner area and, finally, influence its grain size as seen in the cross section of genuine non-melted seed near to the crucible bottom.

One of the most important factors in thermal history, that control the grain size, is the temperature setting of heaters in the furnace. The effect of thermal gradient is only found in the vertical cut due to the vertical heat effect whereas the horizontal cut shows similar grain structure

B. Consequences on ingot grain structure

Combined PL and EBSD results prove that initial growth is governed by nucleation on seed so that the seed layer structure is reproduced at the initial growth interface. This simple but important point implies that the initial grain structure is controlled fully by the seed layer properties. As a consequence, the grain size on the seed layer will control the initial size of the columnar grains. Moreover, the wider the grains in the seed layer, the longer the columnar grains whereas a high density of grain boundaries associated to small grains might be preferred in HPMC-Si process. Another important point is that grain selection is strong in the first 5-millimeter of growth, larger grains having a higher survival probability. Further investigation needs to be conducted to find which kind of initial grain size could generate lower dislocated area in the whole ingot.

In the case of the utilization of poly-Si chunks as seed, the combination of the initial grain size variation and of the different thermal gradient might provide a higher variation of grain size in the seed layer. However, lower grain size variation and a bigger grain size might develop in the re-solidified seed. As the larger initial grains have a higher survival probability, the columnar grains grown from the re-solidified seed can develop longer and can be found at the top part of the ingot. We can expect that an appropriate adjustment between the gradient temperature and the poly-Si size can ensure homogenous grain size. Having homogenous grain size might also have an impact on the occurrence of dislocated areas as observed when using FBR as seed in comparison to the poly-Si chunk seed [7]. From this, we can conclude that we should control the formation of specific grain properties from the seeds to be able to tailor the ingot properties.

Additionally, as the growth initiated from the remaining seed grains, the initial crystallographic orientation is mainly random as expected in the growth of HPMC-Si ingot. This orientation is not promoted only by the genuine non-melted seed, but also by the combination with the re-solidified infiltrated silicon melt seed providing a random orientation base for the HPMC-Si initial growth. The random orientation in the genuine non-melted seed is expected from the initial grain orientation in the poly-Si chunks. The random orientation in the re-solidified infiltrated silicon melt seed is a consequence of the small grains development after arrival of the infiltrated melt in the cold region. These small grains are solidified without preferred orientation and without an assistance from the poly-Si chunk. It leads to a random orientation as in the genuine non-melted seed.

At the start of growth, the occurrence of RAGB and Σ3 boundaries in the vertical section are similar to what is also observed in the literature. This initial growth, in the first 5-milimeter, shows similar length of grain boundary type as found in the seed layer near the growth interface. The RAGB length has the highest proportion above 50% followed by Σ3 boundaries. There are several factors that influence the length of RAGB. As the RAGB grow in the same direction together with the columnar grains, they elongate perpendicular to the growth interface. Oppositely, Σ3 boundaries grow in geometrical directions imposed by the {111} facets with a short growth length [13]. Therefore, the growth length of RAGB is much longer in the initial stage.

However, the Σ3 twin grains are easily formed due to their lowest energy of formation and thus they can be found associated to almost all columnar grains. In the columnar grains, the presence of Σ3 boundaries, which is associated with twin growth, can also be initiated by the seed layer. The grains of the seed layer grow jointly with associated Σ3 twin grains. The Σ3 grain boundaries in the seed layer are not only formed by the re-solidified infiltrated melt seed or during the synthesis of poly-Si chunk in the Siemens process. They can also be formed as twin annealing growth during the coarsening of poly-Si chunk [19]. This coarsening is clearly seen by comparing the microstructure of poly-Si chunk before and after the ingot growth.

V. SUMMARY OF THE WORK

The seed layer morphology from HPMC-Si ingots is found to vary from the bottom of the crucible to the initial growth interface. There are two domain morphologies at the bottom of the seeds: a genuine non-melted seed, and a re-solidified seed. The genuine non-melted seed undergoes a strong grain coarsening generating an increasing grain size toward the growth interface due to the thermal history.

The comparison of PL imaging and EBSD shows that at the seed layer-growth interface, growth takes place on all grains intersecting the growth interface. Consequently, a strong correlation between the seed layer grain sizes and crystallographic orientation exists in the first growth area. Grains are randomly oriented, contain twins and RAGB boundaries with equivalent radial grain size in this region. The larger seed grains regrown at the initial growth interface have a longer survival length. It suggests that the largest grains in the seeds are more prone to generate the final grain structure after further growth.

As a consequence, two major parameters control grain size and grain selection: seed layer formation during the melting stage and the first stage of columnar growth for the given processing parameters. In the future, we will also focus on the grain crystallographic orientation in the propagation length analysis and on the analysis of the dislocation density and distribution related to the seeding.

ACKNOWLEDGMENTS

This work was partially funded by the CEA-INES, France and the Ministry of Research, Technology and Higher Education Republic of Indonesia, through its Scholarship Program for Research and Innovation in Science and Technology (RISET-Pro) World Bank Loan No. 8245-ID. The authors would like to acknowledge N. Plassat and D. Ponthenier for ingot growth.

REFERENCES

[1] C. W. Lan, W. C. Lan, T. F. Lee, A. Yub, Y. M. Yang, W. C. Hsu and A. Yang, "Grain control in directional solidification of photovoltaic silicon," *Journal of Crystal Growth*, vol. 360, pp. 68-75, 2012.

[2] C. W. Lan, C. F. Yang, A. Lan, M. Yang, A. Yu, H. P. Hsu, B. Hsu and C. Hsu," Engineering silicon crystals for photovoltaics," *CrystEngComm*, vol.18, pp. 1474–1485, 2016.

[3] Arjan Ciftja and Gaute Stokkan, "Growth of High Performance Multicrystalline Silicon: A Literature Review," 978-82-14-05742-3, 2014.

[4] Supawan Joonwichien, Satoru Matsushima and Noritaka Usami, "Effects of crystal defects and their interactions with impurities on electrical properties of multicrystalline Si," *Journal of Applied Physics*, vol. 113, pp 133503-1 – 6, 2013.

[5] G. Stokkan, Y. Hub, O. Mios and M. Juel, "Study of evolution of dislocation clusters in high performance multicrystalline silicon," *Solar Energy Materials & Solar Cells*, vol. 130, pp. 679-685, 2014.

[6] R. R. Prakash, T. Sekiguchi, K. Jiptner and Y. Miyamura, "Grain growth of cast-multicrystalline silicon grown from small randomly oriented seed crystal," *Journal of Crystal Growth*, vol. 401, pp. 717-719, 2014.

[7] K. Ekstrøm, G. Stokkan, A. Autruffe, R. Søndenå, H. Dalaker, L. Arnberg and M. D. Sabatino, "Microstructure of multicrystalline silicon seeded by polysilicon chips and fluidized bed reactor granules," *Journal of Crystal Growth*, vol. 441, pp. 95-100, 2016.

[8] T. Trupke, B. Mitchell, J. Weber, W. McMillan and R. Bardos, "Photoluminescence Imaging for Photovoltaic Applications," *Energy Procedia*, vol. 15, pp. 135-146, 2012.

[9] P. Walker and W. H, Eds., CRC Handbook of Metal Etchants, Boca Raton, Florida: CRC Press LLC, 1991.

[10] ASTM E112-12, Standard Test Methods for Determining Average Grain Size, West Conshohocken, PA: ASTM International, 2012.

[11] R. W. Fancher, C. M. Watkins, M. G. Norton, D. F. Bahr, and E. W. Osborne, "Grain growth and mechanical properties in bulk polycrystalline silicon," *Journal of Materials Science*, vol. 36, pp. 5441-5446, 2001.

[12] H. Abrams, "Grain Size Measurement by the Intercept Method," *Metallography*, vol. 4, pp. 59-78, 1971.

[13] M. Tsoutsouva, T. Riberi-Beridot, G. Regula, G. Reinhart, J. Baruchel, F. Guittonneau, L. Barrallier and N. Mangelinck-Noël, "In situ investigation of the structural defect generation and evolution during the directional solidification of ⟨110⟩ seeded growth Si," *Acta Materialia*, vol. 115, pp. 210-223, 2016.

[14] Huntsman Advanced Materials, Araldite® AY 103-1/ Hardener HY 991, March 2009.

[15] Yuzuru Sato et al., "Viscosity of molten silicon and the factors affecting measurement," Journal of Crystal Growth, vol. 249, pp. 404-415, 2003.

[16] M. Trempa, C. Reimann, J. Friedrich, G. Müller, A. Krause, L. Sylla and T. Richter, "Defect formation induced by seed-joints during directional solidification of quasi-mono-crystalline silicon ingots," *Journal of Crystal Growth*, vol. 405, pp. 131 – 141, 2014.

[17] Q. Wang, R. P. Liu, Y. Q. Qian, D. C. Lou, Z. B. Su, M. Z. Ma, W. K. Wang, C. Panofen and D.M. Herlach, "Metal-like growth of silicon during rapid solidification by quenching undercooled droplets on a chill plate," *Scripta Materialia*, vol. 54, pp. 37-40, 2006.

[18] C. Daey Ouwens and H. Heijligers, "Recrystallization processes in polycrystalline silicon," *Applied Physics Letters*, vol. 26, pp. 569-571, 1975

[19] R. E. Smallman and R. J. Bishop, Modern Physical Metallurgy and Materials Engineering: Science, Process, Application, 6th ed., Oxford: Butterworth-Heinemann, 1999.